Engineering a long-acting, potent GLP-1 analog for microstructure-based transdermal delivery

Peng-Yu Yang[a,b,1], Huafei Zou[b,1], Elizabeth Chao[b], Lance Sherwood[b], Vanessa Nunez[b], Michael Keeney[c], Esi Ghartey-Tagoe[c], Zhongli Ding[c], Herlinda Quirino[b], Xiaozhou Luo[a], Gus Welzel[b], Guohua Chen[c], Parminder Singh[c], Ashley K. Woods[b,2], Peter G. Schultz[a,b,2], and Weijun Shen[b,2]

[a]Department of Chemistry and The Skaggs Institute for Chemical Biology, The Scripps Research Institute, La Jolla, CA 92037; [b]California Institute for Biomedical Research, La Jolla, CA 92037; and [c]Corium International, Inc., Menlo Park, CA 94025

Contributed by Peter G. Schultz, February 18, 2016 (sent for review December 24, 2015; reviewed by William F. DeGrado and Marc Montminy)

Antidiabetic treatments aiming to reduce body weight are currently gaining increased interest. Exendin-4, a glucagon-like peptide-1 (GLP-1) receptor agonist administered twice daily via s.c. injection, improves glycemic control, often with associated weight reduction. To further improve the therapeutic efficacy of exendin-4, we have developed a novel peptide engineering strategy that incorporates a serum protein binding motif onto a covalent side-chain staple and applied to the peptide to enhance its helicity and, as a consequence, its potency and serum half-life. We demonstrated that one of the resulting peptides, E6, has significantly improved half-life and glucose tolerance in an oral glucose tolerance test in rodents. Chronic treatment of E6 significantly decreased body weight and fasting blood glucose, improved lipid metabolism, and also reduced hepatic steatosis in diet-induced obese mice. Moreover, the high potency of E6 allowed us to administer this peptide using a dissolvable microstructure-based transdermal delivery system. Pharmacokinetic and pharmacodynamic studies in guinea pigs showed that a single 5-min application of a microstructure system containing E6 significantly improved glucose tolerance for 96 h. This delivery strategy may offer an effective and patient-friendly alternative to currently marketed GLP-1 injectables and can likely be extended to other peptide hormones.

GLP-1 receptor agonist | helix stabilization | half-life extension | microstructure array | lipidated cross-linker

B-family G protein-coupled receptors (GPCRs) include receptors for peptide hormones such as glucagon, glucagon-like peptides 1 and 2 (GLP-1 and -2), parathyroid hormone (PTH), and corticotropin-releasing factor. Attempts to generate small-molecule modulators of these receptors have had limited success, whereas peptide ligands have been proven as effective therapeutic agents, as exemplified by exenatide (aka exendin-4 or Ex-4), a GLP-1 receptor agonist for diabetes, and teriparatide, a PTH1 receptor agonist for osteoporosis (1). However, peptide-based drugs generally suffer from short half-lives due to proteolytic degradation and fast renal clearance, rendering higher doses and frequent injections necessary, which negatively affects patient compliance (2). To improve their pharmacological properties, peptides have been chemically modified by conformational restriction (3–13) to increase potency and reduce proteolysis, and also by lipidation (14–16), polymer conjugation (17–23), and protein fusion (24–26) to decrease renal clearance. Although these latter conjugates can have enhanced circulatory half-lives, they often suffer from reduced potency and, as a result, require injection of relatively large quantities of the modified peptides.

GLP-1 receptor agonists (GLP-1RAs) represent a unique approach to the treatment of diabetes, with benefits beyond glucose control, including favorable effects on body weight, blood pressure, cholesterol levels, and beta-cell function (27). Two short-acting (exenatide and liraglutide; once- or twice-daily administration) and three long-acting (albiglutide, dulaglutide, and exenatide LAR; weekly administration) GLP-1RAs are currently approved in the United States. These drugs mimic the effects of the naturally occurring incretin hormone GLP-1 by activating GLP-1 receptors in the pancreas, which leads to enhanced insulin release and reduced glucagon release in a glucose-dependent manner—with a consequently low risk of hypoglycemia. The effects of these GLP-1RAs on GLP-1 receptors in the CNS and the gastrointestinal tract also lead to reduced appetite and delayed glucose absorption, with concomitant weight loss (28).

Given their limited oral bioavailability, these GLP-1RAs are currently given as an s.c. injection. Transdermal delivery is an attractive alternative because it is relatively noninvasive and painless and avoids the first-pass effect (29). Microstructures, also known as microneedles, are micrometer-scale structures that penetrate the stratum corneum barrier layer of the skin, creating temporary conduits for drugs that cannot passively permeate into the skin due to their large molecular size and hydrophilic nature (30, 31). This technology requires highly potent molecules but offers a number of advantages, including pain-free and simplified administration, and has been successfully evaluated for transdermal delivery of a number of large molecules, including vaccines and human PTH analogs in both preclinical and clinical settings (32, 33). Herein we describe the application of a fatty-acid–derived cysteine side-chain staple to the generation of a highly potent, long-acting Ex-4 analog that shows excellent pharmacokinetics and pharmacodynamics when administered to guinea pigs by dissolvable microstructures.

Significance

Many therapeutic peptides suffer from short plasma half-lives and, as a consequence, require frequent injections to be therapeutically effective; this in turn can adversely affect patient compliance. Here, we describe the development of a novel peptide engineering strategy that incorporates a serum protein binding motif into a covalent side-chain staple. This approach was used to generate stapled long-acting glucagon-like peptide-1 analogs with potency comparable to exendin-4 and significantly enhanced pharmacokinetic properties. Administration by a dissolvable microstructure-based transdermal system resulted in sustained therapeutic blood concentrations with glucose lowering activity in guinea pigs. This approach likely provides a general, straightforward platform for generating stapled long-acting peptide hormones for a range of therapeutic applications.

Author contributions: P.-Y.Y., H.Z., G.C., P.S., A.K.W., P.G.S., and W.S. designed research; P.-Y.Y., H.Z., E.C., L.S., V.N., M.K., E.G.-T., Z.D., H.Q., X.L., G.W., and A.K.W. performed research; P.-Y.Y., H.Z., G.W., G.C., A.K.W., and W.S. analyzed data; and P.-Y.Y., P.G.S., and W.S. wrote the paper.

Reviewers: W.F.D., School of Pharmacy, University of California, San Francisco; and M.M., Salk Institute for Biological Studies.

The authors declare no conflict of interest.

Freely available online through the PNAS open access option.

[1]P.-Y.Y. and H.Z. contributed equally to this work.

[2]To whom correspondence may be addressed. Email: awoods@calibr.org, schultz@scripps.edu, or wshen@calibr.org.

This article contains supporting information online at www.pnas.org/lookup/suppl/doi:10.1073/pnas.1601653113/-/DCSupplemental.

Results and Discussion

Cross-Linker and Peptide Design. Exenatide, a GLP-1 analog originally isolated from the saliva of the Gila monster, has a half-life of 30 min after i.v. administration and a half-life of 2–3 h after s.c. administration in humans (34). Previously, we showed that one could staple two turns of the alpha-helix of oxyntomodulin with a biaryl cross-linker to improve potency and half-life (35). We have further developed this approach with a novel, tunable staple engineered with a serum protein binding motif to significantly improve the potency and serum half-life of the stapled peptide. The crystal structure of Ex-4 (9–39)-NH_2 in complex with the isolated N-terminal domain of GLP-1R (PDB ID code 3C5T) reveals that Ex-4 is a well-defined alpha-helix from residues Leu10 to Asn28, and the receptor binding surface of Ex-4 consists of Glu15, Val19, Arg20, Phe22, Ile23, Leu26, Lys27, and Ser32 (36). We therefore chose the solvent-exposed, paired residues Glu24 and Glu17, Glu24 and Gln13, and Glu24 and Leu10 located on the same face of the alpha-helix to generate the double Cys mutants SEQ-1, SEQ-2, and SEQ-3 spaced at *i* and *i*+7 (two turns: 1.1 nm from *i*), *i* and *i*+11 (three turns: 1.6 nm from *i*), and *i* and *i*+14 (four turns: 2.1 nm from *i*) (Fig. 1 *A* and *B*), respectively. To cross-link the two cysteine residues of SEQ-1, we used the cross-linker *N*, *N*′-butane-1, 4-diyl bis(bromoacetamide) (referred to as L2 herein; *SI Appendix*, Fig. S1). This cross-linker has excellent solubility, is highly selective for thiols, and forms stable thioether adducts (37) (Fig. 1 *C* and *D* and *SI Appendix*, Table S1). The X-ray crystal structure of L2 shows that the Br–Br distance is 11.05 Å (38), which nearly matches the spacing of two turns of a helix. Using L2 as a reference point, we designed a series of cross-linkers with aliphatic or ethylene glycol spacers (L1–L12) to bridge alpha-helical peptides with cysteines spaced at *i*/*i*+7, *i*/*i*+11, or *i*/*i*+14. Incubation of the double Cys mutant (2 mM) with the linker (1.2–1.5 equivalence) in 30 mM NH_4HCO_3 aqueous/CH_3CN (3:1) for 1 h led to >90% conversion to product as determined by LC-MS. Using this approach we rapidly generated a panel of cross-linked peptides, SEQ-1-L1–SEQ-1-L3, SEQ-2-L4–SEQ-2-L7, and SEQ-3-L8–SEQ-3-L10 in ∼75% yield after RP-HPLC purification (*SI Appendix*, Table S2).

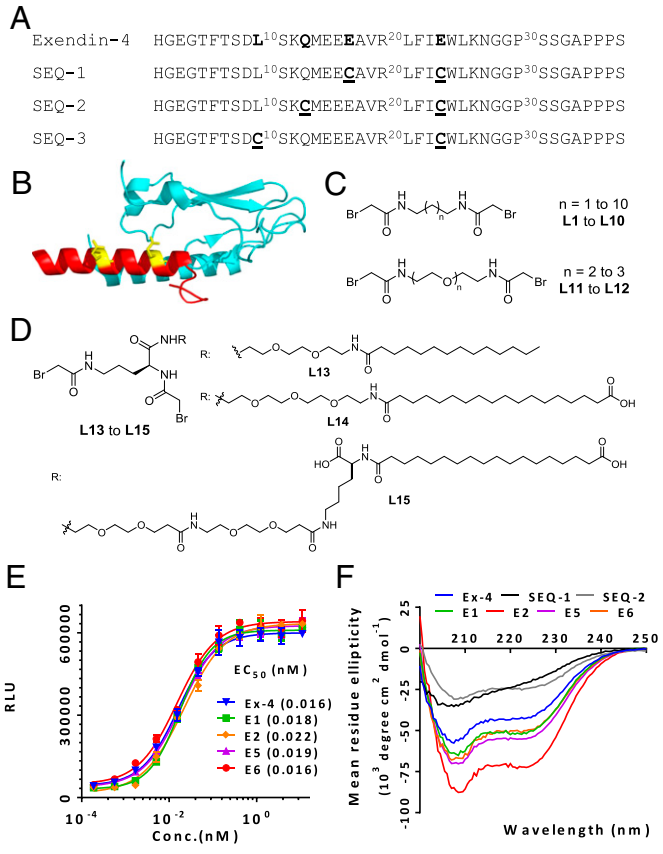

Fig. 1. Design, in vitro activity, and alpha-helicity of cross-linked Ex-4 analogs. (*A*) Sequences of Ex-4 and its double cysteine mutants spaced at *i*, *i*+7; *i*, *i*+11, and *i*, *i*+14. (*B*) Structural model of Ex-4 (9-39) bound to GLP-1 receptor amino-terminal domain (PDB ID code 3C59), with the cross-linking sites colored in yellow. (*C*) Structures of cross-linkers containing bromoacetamide moiety: alkyl-based L1 to L10, PEG-based L11 to L12, and ornithine-derived PEG-fatty acid–based L13 to L15 linkers (*D*). (*E*) In vitro activity of representative cross-linked peptides in the GLP-1R–mediated CRE-Luc reporter assay. (*F*) CD analysis of cross-linked peptides. Data represent mean ± SEM for experiments performed in triplicate.

Receptor-Mediated cAMP Synthesis and CD Spectra. The agonistic activity of these peptides was determined using a cAMP response element (CRE)-driven luciferase reporter in HEK293 cells stably expressing human GLP-1R. Ex-4 was used as a positive control. As summarized in *SI Appendix*, Table S2, introduction of the two Cys residues into the Ex-4 sequence leads to a loss in potency. However, all of the cross-linked peptides showed a significant increase in potency compared with the corresponding noncross-linked peptides. SEQ-3-L9 with the longest bridge (*i*, *i*+14) is somewhat less potent than Ex-4 (EC_{50}s = 150 and 16 pM, respectively), suggesting that the conformational flexibility of this long bridge may not adequately stabilize the helix. Across the entire panel, both the *i*, *i*+7-stapled SEQ-1-L2 (referred to as E1, EC_{50} = 18 pM) and the *i*, *i*+11-stapled SEQ-2-L5 (referred to as E2, EC_{50} = 22 pM) were roughly equipotent to Ex-4. This result indicates that the negatively charged side chains of Glu17 and Glu24 do not contribute significantly to the affinity of Ex-4 for the receptor, nor does the aliphatic cross-linker sterically interfere with receptor binding. Given the similar lengths between the alkyl linker L5–L7 and the PEG2-based linker L11, and between the alkyl linker L8–L10 and the PEG3-based linker L12, we were somewhat surprised to observe a significant loss of activity for the peptides cross-linked with the hydrophilic PEG spaced linkers. It may be that the PEG linkers compete with the amide carbonyl groups for hydrogen bonds to the backbone amide N–H groups of the peptide, or an increase in hydrophilicity disrupts hydrophobic interactions of the amphipathic alpha-helix involved in GLP-1R binding (36).

With these highly potent GLP-1 analogs in hand, next we aimed to improve the pharmacokinetic profile of the *i*, *i*+7-stapled peptide to generate a molecule that is suitable for once-weekly administration. To this end, we took advantage of the well-established strategy of attaching a natural albumin binding moiety (a fatty acid) to the peptide to prolong its duration of action through a "depot" effect [similar to the strategy used for insulin detemir (14) and insulin degludec (15)]. We reasoned that insertion of a short spacer between the fatty acid and the peptide might minimize a loss in agonist potency resulting from albumin binding to the lipid conjugate and sterically interfering with receptor binding. However, given that fatty acid lipophilicity and the position of the carboxylate group could have a significant impact on receptor and albumin binging affinity (39), three different fatty acid analogs were synthesized. These analogs consisted of ornithine linked to myristic acid (C14 acid) or octadecanedioic acid (C18 diacid) via either a triethylene glycol spacer (PEG_3) or a bis-diethylene glycol-lysine (Lys-2xPEG_2) spacer (Fig. 1*D*; see *SI Appendix* for synthesis). The fatty acid-derivatized peptides SEQ-1-L13, SEQ-1-L14, and SEQ-1-L15 (referred to as E3, E5, and E6, respectively) had very high potency even in the presence of 10% FBS. Interestingly, the stapled peptide E6 with a fatty acid side chain retained full agonist activity (EC_{50} = 16 pM), similar to the Ex-4 and wild-type (WT)

GLP-1. Notably, the two regioisomers of E6, which could be easily separated by HPLC, showed very similar potency.

Next we determined the alpha-helicity of the most potent stapled and lipid conjugated peptides by CD using Ex-4 as a positive control. At room temperature, the CD spectra of E1, E5, and E6 (*i*,*i*+7 cross-linked) and E2 (*i*, *i*+11 cross-linked) exhibited a significant increase in alpha-helicity compared with the corresponding uncross-linked peptides SEQ-1 and SEQ-2 (Fig. 1*F*). In particular, SEQ-1 does not form an alpha-helical structure in water. These results suggest that the increased receptor activation results from stabilization of the helical segments by the thioether bridges. Interestingly, the C18 diacid-based cross-linker L15 showed the greatest increase in alpha-helicity, followed by L14 and finally L2, supporting previous reports that lipidation can also stabilize helical structure and modify biological function (40).

Pharmacokinetics and Oral Glucose Tolerance Test in WT Mice. We next determined whether the in vitro potency observed for E1, E5, and E6 translates into better pharmacokinetic (PK) and pharmacodynamic (PD) effects in vivo. The PK properties of Ex-4, E1, E5, and E6 were evaluated in CD1 female mice ($n = 4$ per group) by i.v. or s.c. injection of the peptides (Ex-4: 10 nmol/kg, E1: 7.5 nmol/kg, E5: 7.5 nmol/kg, E6: 7.5 nmol/kg). Peptide concentrations in the plasma at different time points (5 min, 30 min, and 1, 4, 8, and 24 h) were determined using the cell-based receptor activation assay. We noticed significant differences in PK profile of the four peptides. In particular, the maximum concentration in plasma observed 5 min after i.v. dosing is 555 ± 25 nM for E1 compared with 175 ± 12 nM for Ex-4, which is consistent with the short half-life of Ex-4 (~18 min) in mice (*SI Appendix*, Fig. S2 *A* and *B*). Indeed, plasma Ex-4 became undetectable at 1 h. In contrast, the concentration of E1 in plasma remained well above the 5 nM limit of detection method at 4 h, and the half-life is nearly 60 min (*SI Appendix*, Fig. S2 *A* and *B*). As expected, introduction of the C18 diacid in the cross-linker further increased the plasma half-life of the peptides. However, despite having the same C18 diacid, E6 displayed a half-life nearly threefold longer than that of E5 (14 ± 0.2 h vs. 5 ± 0.3 h; Fig. 2*A* and *SI Appendix*, Fig. S2*C*), and the concentration of E6 ranged from 1.5 to 5 times greater than that of E5 at each sample time. The observed time of maximal concentration (T_{max}) of E6 following s.c. administration was ~4 h, similar to that of E5, but the observed maximal plasma concentration (C_{max}) of E6 was 204 ± 5 nM, twofold higher than that of E5 (100 ± 9 nM) (Fig. 2*A* and *SI Appendix*, Fig. S2*C*), which is consistent with the difference of their plasma levels after i.v. dosing. This trend may be related to helical content, particularly in light of the fact that E6 exhibited a far greater alpha-helicity. However, the albumin binding affinity of these peptides remains to be determined and may also play a role. Nonetheless, the serum half-life of E6 is comparable to that of semaglutide (41), which has a dosing frequency of once a week in humans.

Next, we examined the blood-glucose–lowering effect of the optimal peptide E6 in mice ($n = 5$ per group) using an oral glucose tolerance test (OGTT) at multiple time points (15, 30, and 45 min and 1 and 2 h) after single-dose treatment. Vehicle, 10 nmol/kg of Ex-4, or 7.5 nmol/kg of E6 was administered i.v. to the 2-hr-fasted CD1 mice, followed by additional fasting for 6 h before the OGTT. Ex-4 partially decreased blood glucose levels at the time points of 15 and 30 min, whereas E6 markedly decreased blood glucose levels during the entire monitoring period (Fig. 2*B*), which is consistent with the respective plasma half-lives of Ex-4 and E6.

Body Weight Loss in Diet-Induced Obese Mice. Encouraged by the PD results, we used a high-fat-diet–induced obesity (DIO) mouse model to approximate the metabolic effects associated with obesity and type 2 diabetes. We assessed changes in body weight and blood glucose in 14-wk-old DIO mice ($n = 5$ per group) after once-daily i.v. or s.c. treatment for 1 wk (Fig. 2 *C*–*F*). Ex-4

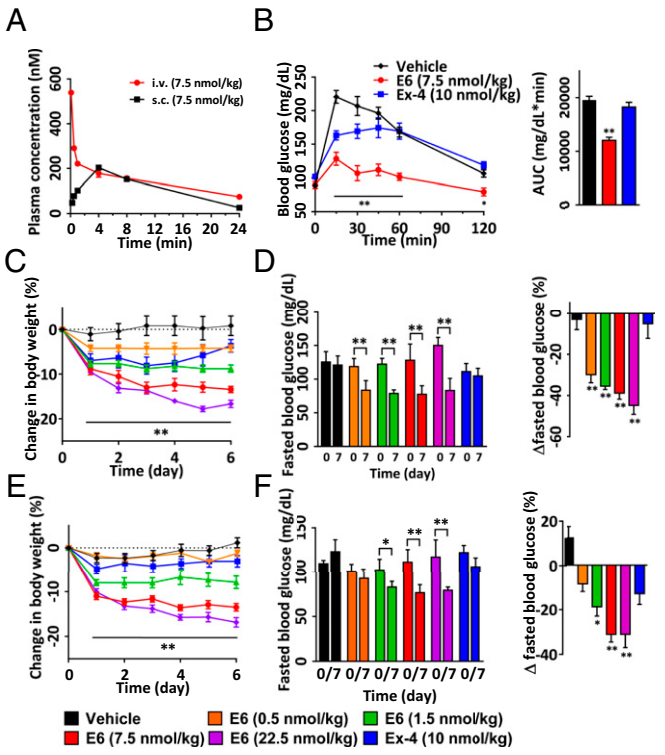

Fig. 2. Pharmacokinetics and OGTT in normal mice, and 1-wk treatment of DIO mice with E6. (*A*) Plasma concentrations of E6 at a dose of 7.5 nmol/kg in CD1 mice ($n = 4$ per group) treated by i.v. or s.c. injection. The peptide concentrations in plasma at various time points were determined by in vitro GLP-1R activity assay. Assay was performed in triplicate. Pharmacokinetic analyses were determined by noncompartmental analysis with WinNonLin. (*B*) Plasma glucose excursion during OGTT in mice ($n = 5$ per group). Mice were i.v. injected with vehicle, E6 (7.5 nmol/kg), or Ex-4 (10 nmol/kg) for 6 h before the glucose challenge. Bar graph showing the level of glucose in the mice obtained by measuring the AUC. (*C*–*F*) Effects of 1-wk i.v. (*C* and *D*) or s.c. (*E* and *F*) treatment of DIO mice ($n = 5$) on body weight change (*C* and *E*) and fasted blood glucose (*D* and *F*). $*P < 0.05$, $**P < 0.01$, E6 vs. vehicle.

(10 nmol/kg, i.v.) did not reduce body weight, whereas E6 caused a significant decrease in body weight in a dose-dependent manner (by −8.8 ± 0.8, −13.4 ± 0.7, and −16.7 ± 0.8% for doses of 1.5, 7.5, and 22.5 nmol/kg, respectively, Fig. 2*C*). Furthermore, E6 significantly protected DIO mice from fasted hyperglycemia at all doses tested compared with Ex-4 (Fig. 2*D*). Importantly, even at a high dose of 22.5 nmol/kg, E6 did not cause hypoglycemia or other side effects. Likewise, reduction in body weight and improvement in glucose homeostasis was observed for E6 when it was dosed s.c. (Fig. 2 *E* and *F*).

To test whether E6 has sustained efficacy in a chronic setting, we treated 25-wk-old DIO mice for 5 wk by s.c. dosing of the peptide. WT lean mice were used as normal controls ($n = 9$ per group). As expected, the treated mice exhibited a steady reduction in body weight and fasting blood glucose levels (Fig. 3 *A* and *B*). At an efficacious dose of 7.5 nmol/kg, the peptide significantly reduced body weight by 25.5 ± 1.9% and 28.8 ± 1.7% (vs. baseline) at day 14 and 36, respectively (Fig. 3*A*). This weight loss occurred with a significant decrease in cumulative food intake (Fig. 3*C* and *SI Appendix*, Fig. S3*C*), which is consistent with previous clinical observations that weight loss induced by GLP-1 is mainly attributed to reduced food intake (42). In addition, the decrease in body weight was accompanied by a significant reduction in visceral fat mass (Fig. 3*G*). This result correlated with the finding that the level of peroxisome proliferator-activated

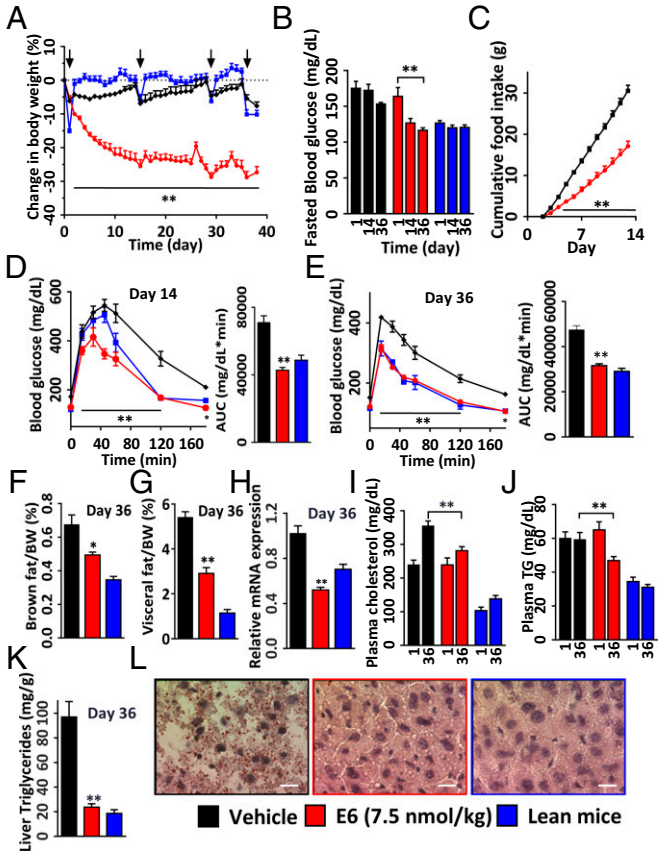

Fig. 3. Five-week treatment of DIO mice with E6 (7.5 nmol/kg s.c.). (*A–L*) Effects on body weight change (*A*), fasted blood glucose on days 14 and 36 (*B*), cumulative food intake (*C*), OGTT on day 14 (*D*), IPGTT on day 36 (*E*), brown fat (*F*) and visceral mass change (*G*), PPAR-gamma mRNA levels in brown fat (*H*), plasma cholesterol (*I*), plasma triglycerides (*J*), liver triglycerides (*K*) of the male DIO mice on day 36 (age 8 mo; $n = 9$ per group), and (*L*) effect on liver steatosis of DIO mice. The arrows indicate time of fasting for glucose tolerance test. $^{*}P < 0.05$, $^{**}P < 0.01$, E6 vs. vehicle. (Scale bars, 100 μm.)

receptor gamma (PPAR-gamma) mRNA in white fat was significantly decreased, as quantified by real-time RT-PCR (Fig. 3*H*). Indeed, it is well established that PPAR-gamma, a transcription factor highly expressed in adipose tissue, plays an important role in glucose homeostasis, lipid metabolism, and regulation of fat mass via adipocyte differentiation (43).

Notably, 2 wk after treatment cessation for the high-dose E6 subgroup ($n = 5$), body weight rebounded to levels comparable to that of vehicle-treated controls (*SI Appendix*, Fig. S3 *A* and *B*), suggesting that the peptide does not cause irreversible toxicity in DIO mice. This notion was further confirmed by analysis of hematology and blood chemistry in which we did not observe any obvious differences between the high-dose and vehicle groups ($n = 4$; *SI Appendix*, Figs. S3 *D* and *E* and S4 *A–E*). In addition, we screened E6 against 168 different GPCR targets in a panel of functional cell-based assays (gpcrMAX;, DiscoveRx). Using strict criteria for a positive result (15% of the activity of the native ligand), we confirmed that E6 displayed no cross-reactivity to any of the receptors other than GLP-1R (*SI Appendix*, Table S3).

In addition to a reduction in fasting blood glucose levels, we also observed improved glucose homeostasis in an oral glucose challenge on day 14 and i.p. glucose tolerance test (IPGTT) on day 36. Blood glucose profiles [peaks and areas under the curve (AUCs)] in the E6-treated group were similar to the control lean mice group and were significantly lower compared with the control vehicle-treated group (Fig. 3 *D* and *E*). To examine potential benefits on lipid metabolism, we assessed changes in triglycerides and cholesterol in DIO mice. E6 treatment resulted in decreased plasma cholesterol level (281 ± 12 mg/dL, compared with vehicle 354 ± 14 mg/dL) and reduced triglyceride levels in both plasma and liver (45 ± 2 and 25 ± 4 mg/dL, respectively) relative to vehicle (59 ± 4 and 87 ± 12 mg/dL, respectively) (Fig. 3 *I–K*). Importantly, chronic treatment with E6 had a significant effect on reducing hepatic lipid content, because the accumulation of lipid droplets in the liver of DIO mice was greatly reduced (Fig. 3*L*). These results suggest that E6 may be useful for the treatment of fatty liver diseases such as nonalcoholic fatty liver disease and nonalcoholic steatohepatitis (44, 45).

Fabrication and Characterization of E6 Peptide Microstructure Arrays. Given the very high potency, the relatively long serum half-life, and the necessity of parenteral administration, E6 is an ideal candidate for microstructure array (MSA)-based transdermal delivery. The MicroCor transdermal delivery system is a microstructure-based platform that incorporates the drug of interest into an array of solid-state, biodegradable microstructures. When these microstructures penetrate the outer layers of the skin, they dissolve rapidly to release the drug for local or systemic uptake. This technology offers painless administration and enhanced safety due to no sharps left after use. Using this platform, we successfully fabricated MSA patches containing peptide E6 that were 16 mm in diameter (2 cm^2 in area) bearing ∼5,800 dissolvable microstructures, as shown in Fig. 4*A* and as described previously (33). The average loading of E6 was 57 μg per 2 cm^2 array. The resulting MSA consisted of a dissolvable drug-in-tip (DIT) layer and a nondissolving, poly(lactic-co-glycolic acid) (PLGA) polymer-based backing layer that connects and supports the MSA tips in the patch. Microscopic inspection of the MSAs revealed sharp, well-formed microstructures (Fig. 4*B*).

To assess the mechanical strength of the microstructures, E6 MSAs were applied in vitro to excised porcine skin and the application sites were then stained with a dye to visualize the penetrations. The microstructures successfully penetrated the skin, resulting in uniform penetration patterns, demonstrating the mechanical robustness of the E6-containing microstructures (Fig. 4*C*). Furthermore, inspections of the MSAs after skin application confirmed that the peptide-containing microstructure tips penetrated and

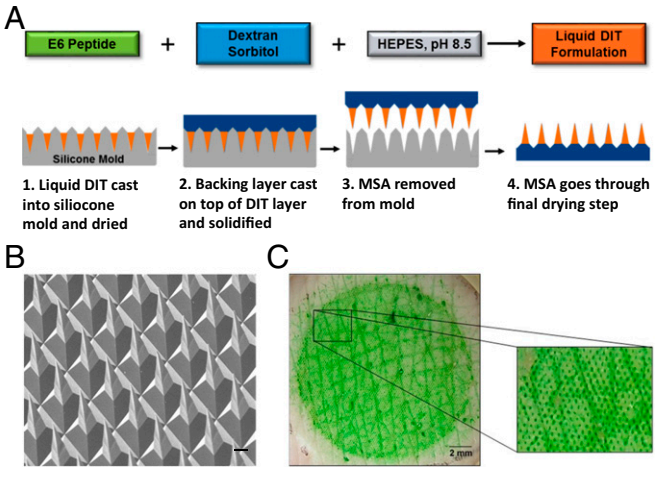

Fig. 4. Fabrication and characterization of MSAs containing E6. (*A*) Schematic of MicroCor fabrication: MSAs were fabricated by casting DIT formulation that contains E6 and excipients into a PDMS mold and drying to form the dissolvable microstructure tips. A PLGA backing layer was then cast and dried over the DIT layer, after which the MSA was removed from the mold. (*B*) SEM image showing the sharp microstructures of a fabricated E6 MSA. (Scale bar, 500 μm.) (*C*) Representative photo of excised porcine skin after a 5-min application of a 2 cm^2 E6 MSA in vitro and then dye staining to highlight the individual penetrations (enlarged view).

dissolved within the skin, leaving behind the stumps of the non-dissolving PLGA backing layer (*SI Appendix*, Fig. S5).

Because room-temperature stability is a key product attribute for both enabling self-administration of microstructure patches and eliminating the need for cold chain management during distribution, we next examined the storage stability of E6 MSAs by reverse-phase ultra-performance liquid chromatography (UPLC). Preliminary data demonstrated that there were no additional peaks observed for the fabricated peptide MSA after being stored at 25 °C for 2 wk or 5 °C for 6 wk (maximum time tested; *SI Appendix*, Fig. S6), indicating that peptide E6 was stable in the MSAs.

PK and PD Evaluation of E6 MSAs in Guinea Pigs. Finally, to investigate transdermal delivery of E6 via the MSAs, PK studies were performed in male Dunkin-Hartley guinea pigs ($n = 4$ per group) after administration of a single target dose of 22.5 nmol/kg via intravenous, s.c. injection, or MSA patch application. Peptide concentrations in the plasma at different time points (5 and 30 min and 1, 2, 3, 5, 8, 24, 32, 48, and 72 h) were determined using the aforementioned in vitro GLP-1R activity assay. A similar pattern of absorption was observed in guinea pigs as in mice after i.v. or s.c. injection. The elimination half-life with i.v. injection was about 16.5 h (*SI Appendix*, Fig. S7). When administered s.c., the plasma concentration of E6 increased gradually for 8 h reaching a C_{max} of 125 ± 7 nM, and then remained well above 10 nM at 72 h postinjection. In comparison, the MSA elicited more rapid systemic absorption of the peptide after a single patch application for 5 min, with T_{max} and C_{max} values of 3 h and 140 ± 21 nM, respectively (Fig. 5*A*). When these microstructures penetrate the outer layers of the skin, they dissolve rapidly to release the drug for systemic uptake, resulting in a faster onset of T_{max} than for s.c. injections. This is consistent with the pharmacokinetics found with MSA delivery of PTH (1-34) and vaccines (32, 33). After quantifying the residual peptide left on the used MSAs and skin surface after each application and subtracting that from the initial drug load in the MSA, the apparent dose delivered for the MSA group was determined to be 45.3 ± 1.8 μg, which had a delivery efficiency of about 80%. Based on dose-normalized AUC, the relative bioavailability of E6 delivered by MSA compared with s.c. injection was greater than 90% using a patch formulation that was not optimized for bioavailability.

We next examined the antidiabetic PD effects of fabricated E6 MSAs by OGTT in male Dunkin-Hartley guinea pigs treated with a MSA patch application to the skin for 5 min in comparison with an s.c. injection dose of 22.5 nmol/kg ($n = 4$ per group). The PD effects were assessed 24 h after treatment by measuring blood glucose levels at multiple time points (5, 15, 30, and 45 min and 1, 2, 3, and 4 h) after oral glucose challenge. As expected, both s.c. injection of E6 and application of an E6 MSA patch significantly lowered blood glucose levels compared with sham administrations (s.c. vehicle and placebo MSA, respectively) at 15, 30, 45, 60, and 120 min postchallenge (Fig. 5 *B* and *C*). Importantly, guinea pigs treated with a single E6 MSA patch displayed sustained control of blood glucose levels (after glucose challenge and fasted glucose) for nearly 4 d after administration, in comparison with animals treated with the placebo MSA (Fig. 5 *C*–*F*). This long-acting effect will likely translate into once-weekly dosing in humans via a single microstructure patch application. We also noted no adverse reactions at the application sites in animals during the course of study, suggesting good local in vivo skin tolerability for E6.

Conclusion

In summary, we have developed a novel peptide engineering strategy that incorporates a serum protein binding motif onto covalent side-chain staple. This approach was used to generate stapled long-acting Ex-4 analogs, which retained full agonist potency and had excellent pharmacological properties, including weight loss, glycemic control, and lipid-lowering effects in rodents.

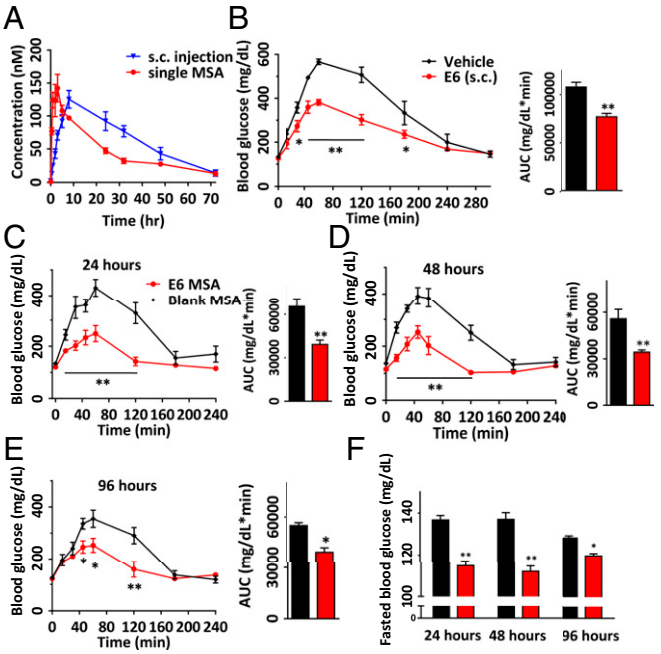

Fig. 5. Pharmacokinetics and OGTT in male Dunkin-Hartley guinea pigs ($n = 4$ per group). (*A*) Plasma concentrations of E6 in guinea pigs treated by s.c. injection or a single MSA at a dose of (22.5 nmol/kg). The peptide concentrations in plasma at various time points were determined by in vitro GLP-1R activity assay. Assay was performed in triplicate. Pharmacokinetic analyses were determined by noncompartmental analysis with WinNonLin. (*B*–*F*) OGTT in guinea pigs after E6 delivery via s.c. injection ($n = 5$) and a single MSA application to skin for 5 min ($n = 4$). s.c. injections of vehicle and 5-min applications of placebo MSAs served as negative controls, respectively ($n = 5$ for both). Plasma glucose excursions during glucose challenge 24 h after s.c. injection of E6 (22.5 nmol/kg) and vehicle (*B*) and 24 h (*C*), 48 h (*D*), and 96 h (*E*) after E6 MSA and placebo MSA applications to skin. (*F*) Fasted blood glucose in guinea pigs at 24 h, 48 h, and 96 h after application of E6 MSA (red) and placebo MSA (black). $*P < 0.05$, $**P < 0.01$, E6 vs. s.c. vehicle or placebo MSA.

Administration by the MicroCor transdermal system resulted in sustained therapeutic blood concentrations with glucose-lowering activity in guinea pigs and warrants further investigation in primates. Expansion of this half-life extension strategy to other peptide hormones, such as GLP-1R/GCGR dual agonists and GLP2, should be technically straightforward.

Methods

Materials and General Procedures. All cysteine mutant peptides and Ex-4 were purchased from Innopep (greater than 95% purity) and Cellmano (greater than 95% purity). In addition to quality-control data supplied with the purchased peptides, all peptides were characterized in-house using electrospray ionization mass spectrometry (ESI-MS). Solvents and chemicals were purchased from the commercial sources and used directly without further purification. ESI-MS was performed on an Agilent G1946C 1100 Series LC-MS system. Peptide purification was performed by preparative RP-HPLC with an Agilent 1260 Infinity Quaternary LC system using a Luna 5u C18 (2) 100A (5 μm, 100 × 30.0 mm) reverse-phase column from Phenomenex with a linear gradient from 20–80% of solvent B for 30 min at a flow rate of 15 mL/min (A, water with 0.1% TFA; B, acetonitrile with 0.1% TFA). Compounds were detected by UV absorption at 220 and 254 nm. The fractions containing the products were freeze dried, and their identity was confirmed by ESI-MS and MALDI-TOF. Analytical HPLC was performed using an Agilent 1100 series LC-MS system with a ZORBAX C18 column (5 μm, 150 × 4.6 mm) from Agilent with a linear gradient of 20–80% of solvent B for 20 min at a flow rate of 1.0 mL/min (A, water with 0.05% TFA; B, acetonitrile with 0.05% TFA) with UV/vis spectrometric detector with wavelength set at 220 and 254 nm.

Animals and Statistical Analysis. All animal care and experimental procedures were approved by the Institutional Animal Care and Use Committee (IACUC)

of the California Institute for Biomedical Research (Calibr), La Jolla, CA and strictly followed the NIH guidelines for humane treatment of animals. The results are expressed as means ± SE, and the data were compared using the unpaired Student's *t* test. Where appropriate, data were compared using repeated measures or one-way analysis of variance, followed by the Student–Newman–Keuls post hoc test. Incremental AUC analyses for plasma glucose was calculated using GraphPad Prism 6. Groups of data were considered to be significantly different if $P < 0.05$.

Fabrication of E6 Peptide MSAs. A DIT solution was formulated by dissolving E6, Dextran 70, and sorbitol in 10 mM Hepes buffer, pH 8.5. The liquid DIT formulation was then cast into negative molds made of polydimethylsiloxane (PDMS) (Fig. 4*A*, step 1). The DIT formulation was dried under controlled temperature conditions (20–35 °C) to form the DIT layer (Fig. 4*A*, step 1). A solution of PLGA was then cast on top of the dried DIT layer to form a non-water-soluble backing layer that connects and supports the DIT layer microstructure tips (Fig. 4*A*, step 2). A polycarbonate film was laminated on top of the dried PLGA backing with adhesive. MSA was formed by delaminating the construct from the PDMS mold (Fig. 4*A*, step 3). At this point, circular MSAs of the desired size, 16 mm in diameter (area 2 cm^2), were die-cut from the larger array and inspected under a stereomicroscope to ensure good microstructure formation and sharp tips. The final microstructures are four-sided pyramids, ∼200 μm long, with a center-to-center spacing of ∼200 μm, and a density of ∼2,900 microstructures per cm^2. After inspections, the die-cut MSAs were further dried to remove residual moisture (Fig. 4*A*, step 4) before being heat-sealed in foil pouches in a nitrogen-filled isolator. Unless otherwise noted, pouched MSAs were stored at 2–8 °C until use.

In Vivo Application of MSAs in Guinea Pigs for PK and PD Studies. Male Dunkin-Hartley guinea pigs weighing ∼400 g were obtained from Charles River Laboratories and used to test the PK and PD of the E6 MSAs. To prepare the animals for MSA applications, the hair on the back and sides of each animal was removed by clipping and careful shaving. The arrays were then applied to a flap of dorsal skin using the same spring-based applicator described previously (33). Five minutes after application, the MSA was removed from the skin and retained for analysis of residual peptide. Fifteen minutes after MSA removal, the skin was lightly swabbed to collect any residual peptide remaining on the skin. The used MSAs and skin swabs were assayed for residual E6 peptide by reverse-phase UPLC; based on these results and the initial drug load, the apparent dose delivered for the E6 MSAs was determined.

For the PK study in guinea pigs, animals were dosed with E6 by i.v. injection, s.c. injection, or a 5-min application of an E6 MSA to the skin ($n = 4$ per group). For each group, the peptide was administered at a target dose level of 22.5 nmol/kg. Blood was extracted at different time points (5 and 30 min and 1, 2, 3, 5, 8, 24, 32, 48, and 72 h postdosing) and peptide concentration in the plasma was determined by in vitro GLP-1R activity assay as described in the *SI Appendix*. The relative bioavailability was calculated as the ratio of dose-normalized AUC between MSA application and s.c. injection groups.

For the PD study in guinea pigs, animals ($n = 4$ per group) were fasted for 4 h and treated with a MSA patch (a placebo MSA as negative control) application to the skin for 5 min. After 24, 48, and 96 h, animals were orally administrated with 2 g of glucose solution per kg of body weight and their blood glucose levels were measured before (0 min) and after glucose challenge for the indicated time point.

1. Lagerström MC, Schiöth HB (2008) Structural diversity of G protein-coupled receptors and significance for drug discovery. *Nat Rev Drug Discov* 7(4):339–357.
2. Fosgerau K, Hoffmann T (2015) Peptide therapeutics: Current status and future directions. *Drug Discov Today* 20(1):122–128.
3. Jackson DY, King DS, Chmielewski J, Singh S, Schultz PG (1991) General approach to the synthesis of short alpha-helical peptides. *J Am Chem Soc* 113(24):9391–9392.
4. Leduc AM, et al. (2003) Helix-stabilized cyclic peptides as selective inhibitors of steroid receptor-coactivator interactions. *Proc Natl Acad Sci USA* 100(20):11273–11278.
5. Shepherd NE, Hoang HN, Abbenante G, Fairlie DP (2005) Single turn peptide alpha helices with exceptional stability in water. *J Am Chem Soc* 127(9):2974–2983.
6. Harrison RS, et al. (2010) Downsizing human, bacterial, and viral proteins to short water-stable alpha helices that maintain biological potency. *Proc Natl Acad Sci USA* 107(26):11686–11691.
7. Muppidi A, et al. (2012) Rational design of proteolytically stable, cell-permeable peptide-based selective Mcl-1 inhibitors. *J Am Chem Soc* 134(36):14734–14737.
8. Walensky LD, et al. (2004) Activation of apoptosis in vivo by a hydrocarbon-stapled BH3 helix. *Science* 305(5689):1466–1470.
9. Chang YS, et al. (2013) Stapled α-helical peptide drug development: A potent dual inhibitor of MDM2 and MDMX for p53-dependent cancer therapy. *Proc Natl Acad Sci USA* 110(36):E3445–E3454.
10. Walensky LD, Bird GH (2014) Hydrocarbon-stapled peptides: Principles, practice, and progress. *J Med Chem* 57(15):6275–6288.
11. Chongsiriwatana NP, et al. (2008) Peptoids that mimic the structure, function, and mechanism of helical antimicrobial peptides. *Proc Natl Acad Sci USA* 105(8): 2794–2799.
12. Cheloha RW, Maeda A, Dean T, Gardella TJ, Gellman SH (2014) Backbone modification of a polypeptide drug alters duration of action in vivo. *Nat Biotechnol* 32(7): 653–655.
13. Johnson LM, et al. (2014) A potent α/β-peptide analogue of GLP-1 with prolonged action in vivo. *J Am Chem Soc* 136(37):12848–12851.
14. Havelund S, et al. (2004) The mechanism of protraction of insulin detemir, a long-acting, acylated analog of human insulin. *Pharm Res* 21(8):1498–1504.
15. Drab SR, Philis-Tsimikas A (2014) A new option for glycemic control: Insulin degludec, a new-generation basal insulin with an ultralong duration of action. *Pharmacotherapy* 34(3):291–302.
16. Penchala SC, et al. (2015) A biomimetic approach for enhancing the in vivo half-life of peptides. *Nat Chem Biol* 11(10):793–798.
17. Harris JM, Chess RB (2003) Effect of pegylation on pharmaceuticals. *Nat Rev Drug Discov* 2(3):214–221.
18. Knop K, Hoogenboom R, Fischer D, Schubert US (2010) Poly(ethylene glycol) in drug delivery: Pros and cons as well as potential alternatives. *Angew Chem Int Ed Engl* 49(36):6288–6308.
19. Verhoef JJF, Anchordoquy TJ (2013) Questioning the use of PEGylation for drug delivery. *Drug Deliv Transl Res* 3(6):499–503.
20. Kopeček J (2013) Polymer-drug conjugates: Origins, progress to date and future directions. *Adv Drug Deliv Rev* 65(1):49–59.
21. Mitragotri S, Burke PA, Langer R (2014) Overcoming the challenges in administering biopharmaceuticals: Formulation and delivery strategies. *Nat Rev Drug Discov* 13(9): 655–672.
22. Schellenberger V, et al. (2009) A recombinant polypeptide extends the in vivo half-life of peptides and proteins in a tunable manner. *Nat Biotechnol* 27(12):1186–1190.
23. Ding S, et al. (2014) Multivalent antiviral XTEN-peptide conjugates with long in vivo half-life and enhanced solubility. *Bioconjug Chem* 25(7):1351–1359.
24. Jimenez-Solem E, Rasmussen MH, Christensen M, Knop FK (2010) Dulaglutide, a long-acting GLP-1 analog fused with an Fc antibody fragment for the potential treatment of type 2 diabetes. *Curr Opin Mol Ther* 12(6):790–797.
25. Zhang Y, et al. (2015) Rational design of a humanized glucagon-like peptide-1 receptor agonist antibody. *Angew Chem Int Ed Engl* 54(7):2126–2130.
26. Liu T, et al. (2015) Functional human antibody CDR fusions as long-acting therapeutic endocrine agonists. *Proc Natl Acad Sci USA* 112(5):1356–1361.
27. Meier JJ (2012) GLP-1 receptor agonists for individualized treatment of type 2 diabetes mellitus. *Nat Rev Endocrinol* 8(12):728–742.
28. Donnelly D (2012) The structure and function of the glucagon-like peptide-1 receptor and its ligands. *Br J Pharmacol* 166(1):27–41.
29. Prausnitz MR, Langer R (2008) Transdermal drug delivery. *Nat Biotechnol* 26(11): 1261–1268.
30. Prausnitz MR (2004) Microneedles for transdermal drug delivery. *Adv Drug Deliv Rev* 56(5):581–587.
31. Sullivan SP, et al. (2010) Dissolving polymer microneedle patches for influenza vaccination. *Nat Med* 16(8):915–920.
32. Wendorf JR, et al. (2011) Transdermal delivery of macromolecules using solid-state biodegradable microstructures. *Pharm Res* 28(1):22–30.
33. Bonificio A, et al. (2015) Fabrication of cell culture-derived influenza vaccine dissolvable microstructures and evaluation of immunogenicity in guinea pigs. *Vaccine* 33(25):2930–2938.
34. Nielsen LL, Baron AD (2003) Pharmacology of exenatide (synthetic exendin-4) for the treatment of type 2 diabetes. *Curr Opin Investig Drugs* 4(4):401–405.
35. Muppidi A, et al. (2016) Design of potent and proteolytically stable oxyntomodulin analogs. *ACS Chem Biol* 11(2):324–328.
36. Runge S, Thøgersen H, Madsen K, Lau J, Rudolph R (2008) Crystal structure of the ligand-bound glucagon-like peptide-1 receptor extracellular domain. *J Biol Chem* 283(17):11340–11347.
37. Lyon RP, et al. (2014) Self-hydrolyzing maleimides improve the stability and pharmacological properties of antibody-drug conjugates. *Nat Biotechnol* 32(10):1059–1062.
38. Martínez-Palau M, Urpí L, Font-Bardia M, Puiggalí J (2005) N,N′-Butane-1,4-diylbis(bromoacetamide). *Acta Crystallogr C* 61(Pt 6):o345–o347.
39. Madsen K, et al. (2007) Structure-activity and protraction relationship of long-acting glucagon-like peptide-1 derivatives: Importance of fatty acid length, polarity, and bulkiness. *J Med Chem* 50(24):6126–6132.
40. Ward BP, et al. (2013) Peptide lipidation stabilizes structure to enhance biological function. *Mol Metab* 2(4):468–479.
41. Lau J, et al. (2015) Discovery of the once-weekly glucagon-like peptide-1 (GLP-1) analogue Semaglutide. *J Med Chem* 58(18):7370–7380.
42. Baggio LL, Drucker DJ (2014) Glucagon-like peptide-1 receptors in the brain: Controlling food intake and body weight. *J Clin Invest* 124(10):4223–4226.
43. Savage DB (2005) PPAR gamma as a metabolic regulator: Insights from genomics and pharmacology. *Expert Rev Mol Med* 7(1):1–16.
44. Eguchi Y, et al.; Japan Study Group for NAFLD (JSG-NAFLD) (2015) Pilot study of liraglutide effects in non-alcoholic steatohepatitis and non-alcoholic fatty liver disease with glucose intolerance in Japanese patients (LEAN-J). *Hepatol Res* 45(3):269–278.
45. Kenny PR, et al. (2010) Exenatide in the treatment of diabetic patients with non-alcoholic steatohepatitis: A case series. *Am J Gastroenterol* 105(12):2707–2709.